Electronic Supplementary Information

Synthesis, Characterization and enhanced Bactericidal action of Chitosan supported Core shell Copper-Silver Nanoparticle Composites

Sadhucharan Mallick, [a] Pallab Sanpui, [a] Siddhartha Sankar Ghosh,[bc] Arun Chattopadhyay [ac] and Anumita Paul [a] *

[a] Department of Chemistry, [b] Department of Biotechnology, [c] Centre for Nanotechnology, Indian Institute of Technology Guwahati, Guwahati 781039, India. *E-mail: anumita@iitg.ernet.in*

TEM of CS-Cu NPs seed particles

Seed Cu NPs were synthesized in presence of CS under normal atmospheric conditions by the alkaline reduction of $CuSO_4$ with hydrazine. The red solid so obtained was isolated from the reaction mixture and dispersed in an aqueous acetic acid solution. TEM images of these CS-Cu NPs are shown in Figure S1.

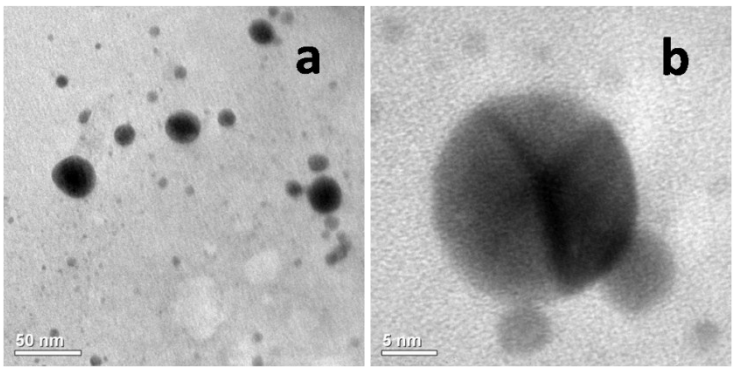

Figure S1 (a) TEM and (b) HRTEM image of freshly prepared CS-Cu NPs seeds.

Table S1. Lattice plane spacings (d-spacings) calculated from the SAED pattern shown in Fig. 2c compared with theoretical values.

Lattice Planes	Experimental	Theoretical
Ag(100)	3.90Å	4.08Å
Ag(110)	2.96Å	2.88Å
Ag(111)	2.21Å	2.35Å
Ag(200)	1.99Å	2.04Å
Ag(220)	1.47Å	1.44Å
Cu(100)	3.67Å	3.61Å
Cu(110)	2.48Å	2.55Å
Cu(111)	2.06Å	2.08Å
Cu(200)	1.77Å	1.80Å
Cu(220)	1.36Å	1.27Å

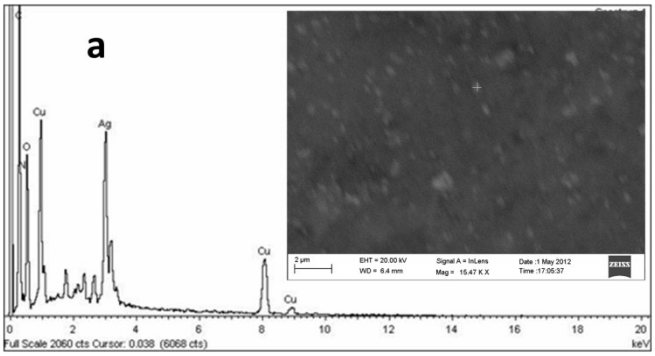

Element	Weight%	Atomic% b
C K	27.52	56.56
N K	3.24	5.71
O K	13.41	20.69
Cu K	26.72	10.38
Ag L	29.11	6.66
Totals	100.00	

Figure S2. (a) Spot EDX spectra, focused on a single Cu@Ag nanoparticle, during FESEM analysis shows the presence of elemental Cu and Ag. Inset shows corresponding FESEM image. (b) Spot EDX result, (spot size 35 nm) given in tabular form.

X-ray diffraction studies

The X-ray diffraction (XRD) pattern of freshly prepared CS-Cu@Ag NPs, shown in Figure S2a, confirmed the formation of face-centered cubic (FCC) lattice of Ag(0) in the composite. The XRD diffraction peaks of the composite matched well with that of metallic Ag (JCPDS-04-0783) except that the 2θ values were slightly shifted to higher values indicating a slight decrease in lattice constant for the shell Ag metal; while the core Cu metal being in kinematic diffraction state, its XRD peaks were not visible. At low coverage the growth of Ag on Cu NPs is epitaxial. But as thickness of Ag shell increases, the lattice mismatch parameter generates large strain in the core Cu metal. This strain is released by breaking up the perfect Cu lattice into imperfect Cu lattices giving an incoherent interface between the core and shell metals, leaving the Ag shell in a dynamical diffraction state and the Cu core in a kinematic diffraction state. [1] The kinematic diffraction state of the core Cu NPs broadens its XRD peaks which are not visible in Figure S2a. In this regard, it may be noted that the XRD pattern of CS-Cu NPs seed particles (Figure S2b), used for the preparation of the CS Cu@Ag NPs composite, showed peaks due to reflection from FCC crystal structures of Cu(0). The calculated lattice parameter of Ag in the CS-Cu@Ag NPs composite is 0.4081 nm in contrast to bulk Ag which is 0.4086 nm and to Ag in CS-Ag NPs which is 0.4071 nm.[2,3] The calculated lattice parameter of seed CS-Cu NPs is 0.3606 nm compared to bulk Cu which is 0.3610 nm.

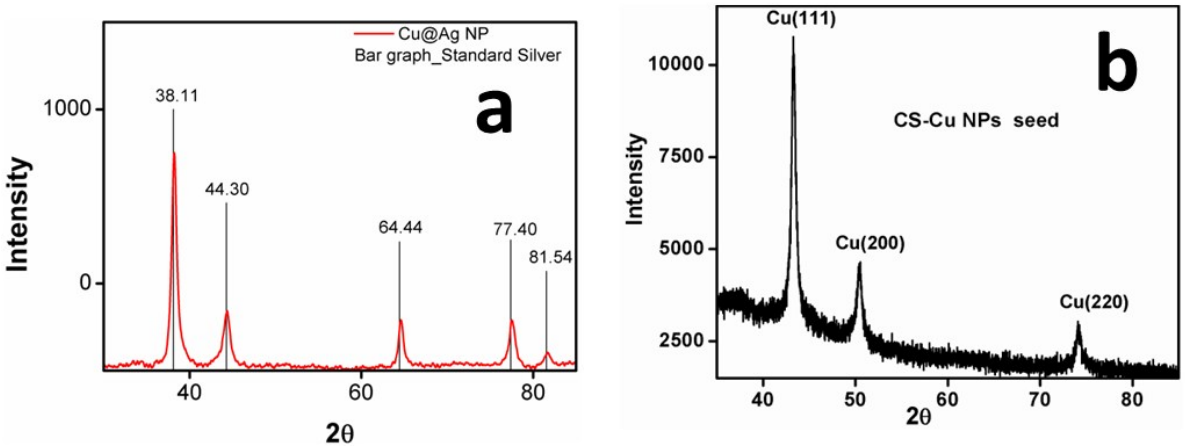

Figure S3. (a) XRD pattern of freshly synthesized CS-Cu@Ag NPs composite and its comparison with standard planes of pure Ag (JCPDS-04-0783) marked by vertical lines. (b) XRD pattern of CS-Cu NPs seed particles.

FTIR Spectroscopy

In the FTIR spectrum of CS, the peaks (Fig. S4) at 1418 cm^{-1} and 1383 cm^{-1} are assigned to the CH_3 symmetrical deformation mode while the 1314 cm^{-1} is assigned to C-N stretching vibration in N-acetyl glucosamine unit. The broad peak at 3434 cm^{-1} is characteristic of N−H stretching and O-H stretching vibrations, while the peak at 1644 cm^{-1} is attributed to carbonyl (-C=O) stretching band of the $CONH_2$ group for native CS. The observed shift from 3434 cm^{-1} to 3428 cm^{-1} and a shift of 1644 cm^{-1} to 1639 cm^{-1} along with band broadening indicates that amino ($-NH_2$) and hydroxyl (-OH) groups of CS are involved to stabilized Cu@Ag nanoparticles in the CS Cu@Ag NPs composite. Further, the peak at 1080 cm^{-1}, in native CS, shifted to 1067 cm^{-1} in CS stabilized Cu@Ag NPs, indicating the interaction between CS matrix and metal nanoparticle (Cu@Ag).

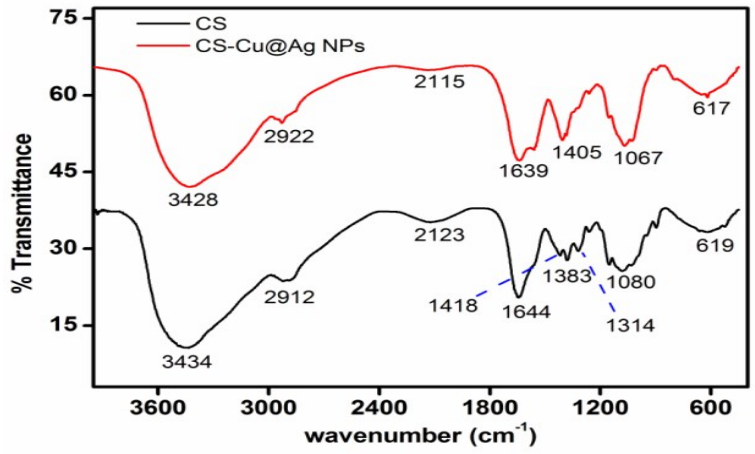

Figure S4 FTIR spectra of CS and CS-Cu@Ag NPs composite.

Stability of CS-Cu@Ag NPs composite kept in air for longer period of time

Fig. S5a shows the time evolution UV-visible spectra of a freshly prepared sample of CS Cu@Ag NPs. The plasmon resonance peak intensity at 417 nm decreases slowly in 15 days, indicating that CS Cu@Ag NPs were stable for at least 15 days in aqueous solution under ambient conditions. XRD pattern of 15 days old sample also showed reflections from fcc crystal planes of Ag (0) (Fig. S5b).

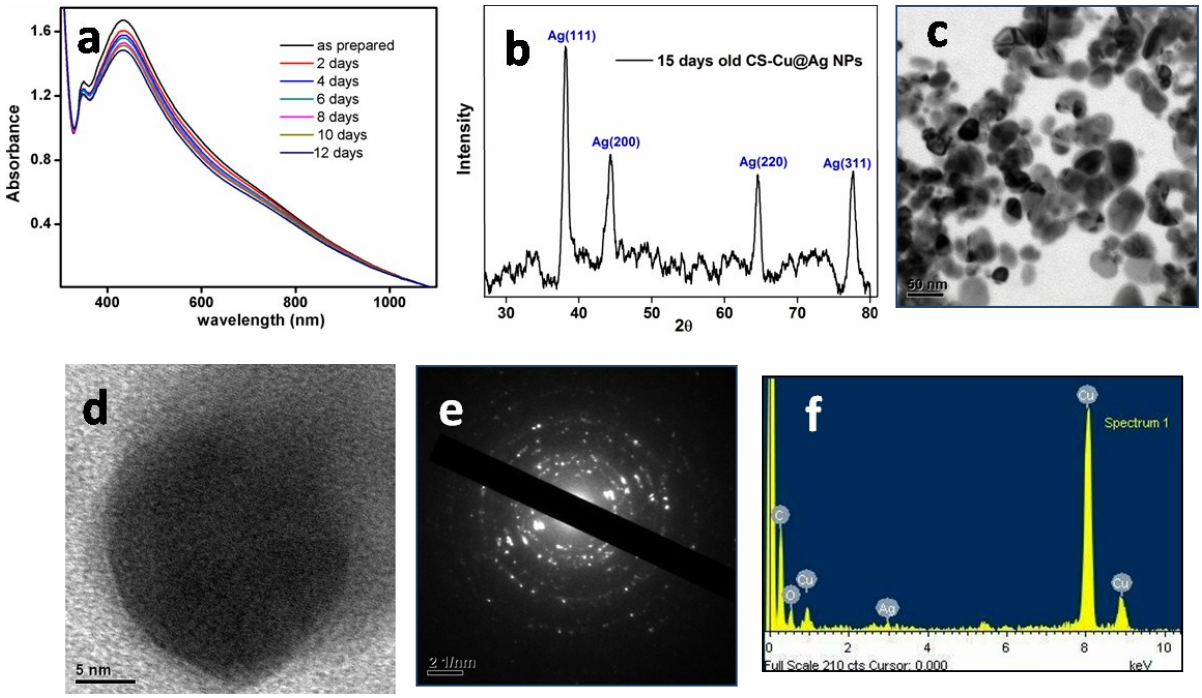

Figure S5 (a) UV-Vis spectra of CS Cu@Ag NPs solution aged to different times as indicated. (b) X-ray diffraction pattern of 15 days old CS-Cu@Ag NPs composite. (c) TEM, (d) HRTEM image **(e)** Selected area diffraction (SAED) pattern of of 20 days old CS Cu@Ag nanoparticles (f) EDX result of CSCu@Ag NPs composite shows presence of elemental copper and silver.

XPS analysis of CS Cu@Ag NPs composite

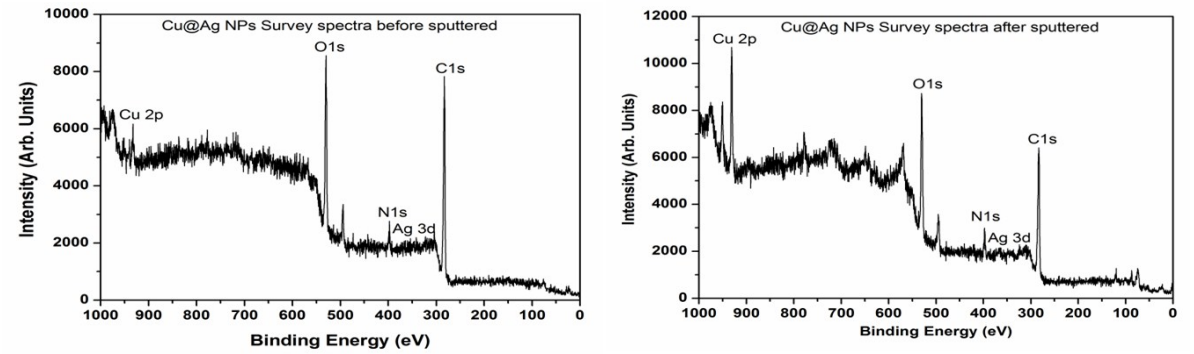

Figure S6 Wide-scan XPS survey spectra of CS Cu@Ag NPs composite samples before and after sputtering.

Studies on antibacterial properties of CS-Cu@Ag NPs composite

To understand the role of each component in the antibacterial properties of the CS Cu@Ag NPs (MIC) sample, we pursued growth curve studies of several samples at different concentrations as shown in Fig. S7a. We examined bactericidal activity of two components system CS-Cu NPs, CS-Ag NPs composites and bare Cu@Ag NPs as well as individual constituents of the composite chitosan, Cu NPs, and Ag NPs only. The results indicated that single components Cu NPs (3.03 µg/mL), Ag NPs (1.47 µg/mL) did not inhibit bacterial growth . CS (58.90 µg/mL) and that two components system CS-Cu NPs, CS-Ag NPs composites and bare Cu@Ag NPs samples showed limited antibacterial properties. The CS Cu@Ag NPs composites at concentrations 63.40 µg/mL (MIC) had retarded bacterial growth populations completely in addition 92.99 µg/mL (MBC) of CS Cu@Ag NPs composites was enough to kill bacteria. We had also seen the complete growth inhibition and killing of Gram-positive *B. cereus* bacteria in presence of CS Cu@Ag NPs composites at 75.46 µg/mL (MIC) and 98.74 µg/mL (MBC) concentrations Fig. S7b. Further the MIC and MBC values for Gram-positive *B. cereus* bacteria were to some extent greater than for the Gram negative *E. coli* bacteria.

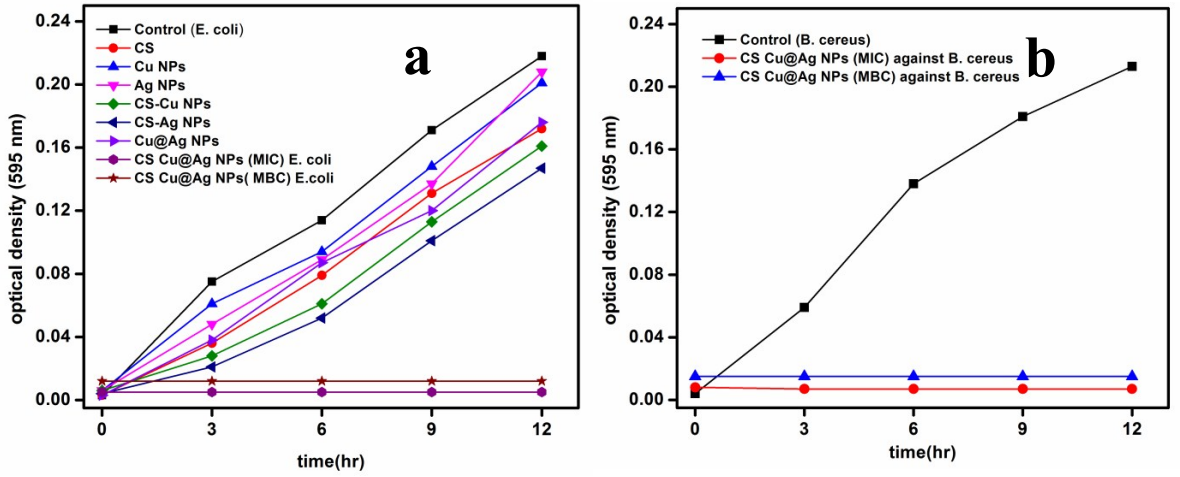

Figure S7. (a) Growth curve of GFP recombinant *E. coli* in the presence of the following: **Control**: 0.02 M acetic acid only in LB media; **CS**: Chitosan at 58.9 µg/mL, **Cu NPs**: Cu NPs at 3.03 µg/mL; **Ag NPs**: Ag NPs at1.47 µg/mL. **CS-Cu NPs**: CS-Cu NPs composite at 62.00 µg/mL; **CS-Ag NPs**: CS-Ag NPs composite at 60.4 µg/mL; **Cu@Ag NPs**: Cu@Ag NPs composite at 4.60 µg/mL**; CS Cu@Ag NPs (MIC):** CS Cu@Ag NPs composite at 63.4 µg/mL**; CS Cu@Ag NPs (MBC):** CS Cu@Ag NPs composite at 92.99 µg/mL **Fig. (b)** Growth curve of Gram-positive *B. cereus* bacteria in the presence of CS Cu@Ag NPs composite: **Control:** 0.02 M acetic acid only in NB media**; CS Cu@Ag NPs (MIC):** CS Cu@Ag NPs composite at 75.46 µg/mL**; CS Cu@Ag NPs (MBC):** CS Cu@Ag NPs composite at 98.74 µg/mL.

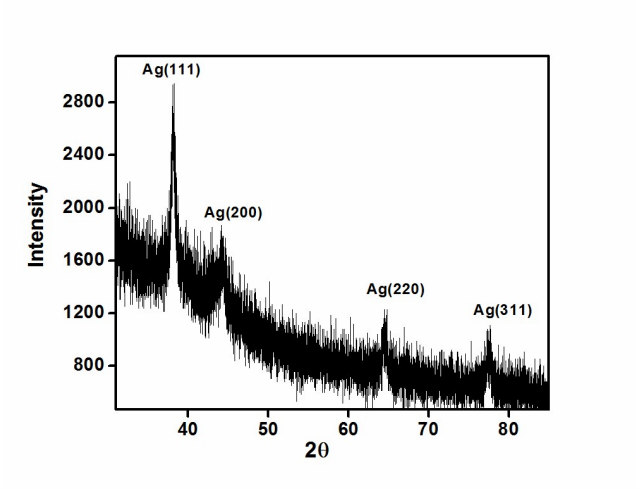

Figure S8. Powder XRD pattern of the centrifuged sample of *E. coli* bacteria obtained following treatment with CS Cu@Ag NPs composite (at its MIC dose) for 12 h.

Interaction of CS-Cu@Ag NPs composite with cell wall

Presence of NPs was ascertained from the dark spots in the TEM images of freshly prepared CS Cu@Ag NPs (**Fig. S9a**) composite and CS Cu@Ag NPs composite samples attached to *E. coli* cell wall (**Fig. S10a, b**). The size distribution of the Cu@Ag NPs in the above two cases, shown in **Fig. S9b** and **S10c**, indicate that the size distribution of the NPs did not change upon attachment of the composite to the bacterial cell membrane.

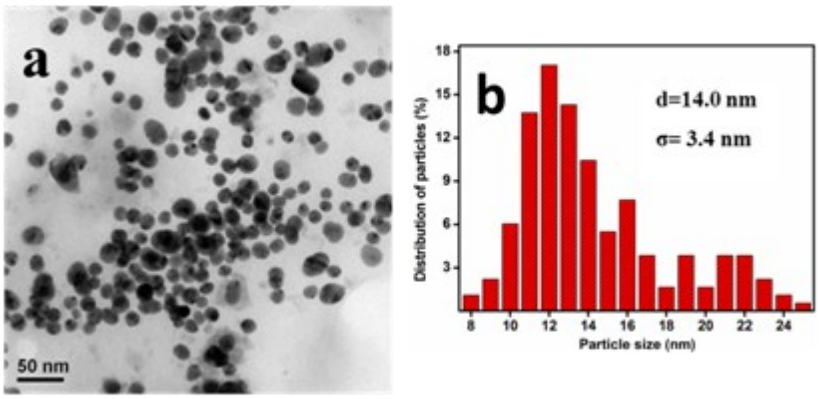

Figure S9 (a) TEM image of freshly prepared CS Cu@Ag NPs and (b) size distribution from image a. The average size is 14.0 ± 3.4 nm.

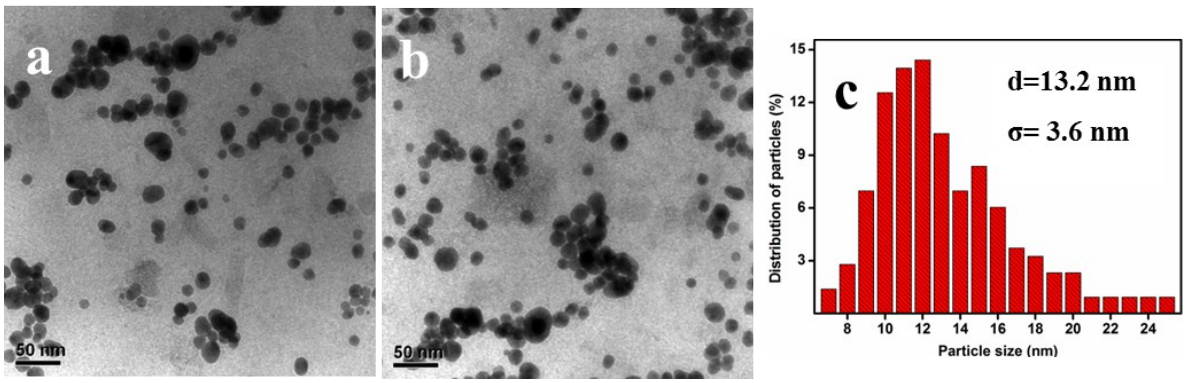

Figure S10 (a,b) TEM images of CS Cu@Ag NPs attached on *E. coli* bacteria cell membrane and (c) size distribution from image a and b. The average size is 13.2±3.6 nm. To get a statistically significant number of particles, the distribution was obtained from two different images captured at two different locations of the same bacterium sample.

Effect of CS Cu@Ag NPs composite on the bacterial DNA

The interaction between DNA and CS Cu@Ag was further studied by agarose gel electrophoresis where recombinant GFP plasmid (pGFP) from the *E. coli* (control) and CS Cu@Ag NPs treated *E. coli* samples were isolated by an alkaline lysis method at different time points and subjected to analysis. Gel retardation assay of isolated pGFP, incubated for 2 h with varying concentration of CS, and CS Cu@Ag NP composite, are reported in **Fig. S11a**. The absence of any band in lane 2 and 3 in Fig. S9a confirmed the complexation of pGFP with CS, as this stopped the movement of the pGFP from the wells. Control sample containing free pGFP (lane 1) shows no such restriction of movement. Likewise, partial retardation in lane 4 and almost complete retardation in lane 5 of pGFP movement is observed on increasing the concentration of CS Cu@Ag NPs composite, confirming the electrostatic nature of complexation of pGFP with the CS Cu@Ag NPs composite. In agarose gel electrophoresis experiment (Fig. S11a) the migration of pDNA in CS treated samples was stopped as the charge density of CS is large. On the other hand, the reduced charge density of CS Cu@Ag NPs results in partial movement of the pGFP in lanes 4 and 5, the extent of which depends on the relative amount of the composite present. The results in **Fig. S11b** similarly show the migration pattern of pGFP isolated from both control and composite treated *E. coli* samples. The pattern in lane 2 and 3 for CS Cu@Ag NPs treated *E. coli* are similar to those of control in lane 1, implying that the composite had no apparent effect on DNA degradation.

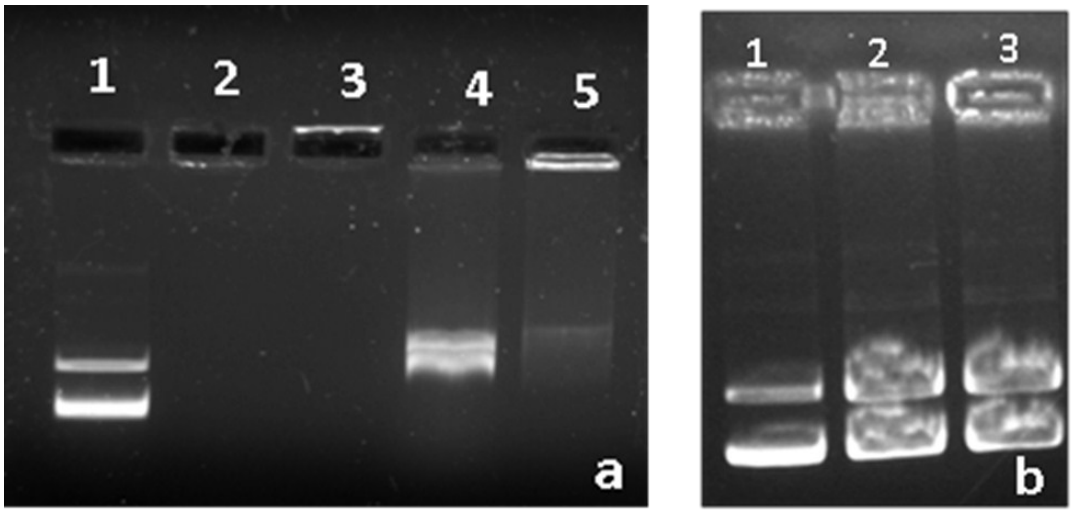

Figure S11 (a) Gel retardation assay of isolated pGFP (0.5 µg in 20 µL reaction volume) incubated for 2 h with varying concentration (1.8, 3.6 µg) of CS (lanes 2, 3) and with varying concentration (1.98, 3.96 µg) of CS Cu@Ag NPs composite (lanes 4, 5). Lanes 1 corresponds to pGFP only (control). (b)Agarose gel electrophoresis of pGFP isolated from *E. coli* cells treated with 3.4 µg/mL of CS Cu@Ag NPs composite. Lane 1: control; Lane 2: 2hr treatment; Lane 3: 4hr treatment.

References

1 J. Zhao, D. Zhang, J. Zhao, *J. Solid State Chem.* 2011**,** ***184,*** 2339.

2 P. Sanpui, A. Chattopadhyay, S. S. Ghosh , *ACS Appl. Mater. Interfaces* 2011**,** ***3,*** 218**.**

3 Z. Chen, X. Zhang, H. Cao, Y. Huang, *Analyst* 2013, ***138,*** 2343.